



Special Feature: Energy Conversion and Storage

Research Report

Density Functional Theory Calculations on Interfacial Electrochemistry

Ryosuke Jinnouchi, Kensaku Kodama, Eishiro Toyoda and Yu Morimoto

Report received on Jun. 26, 2013

ABSTRACT Recent developments and applications of density functional theory combined with a modified Poisson-Boltzmann theory (DFT-MPB) are reviewed. After a brief introduction of conventional DFT calculations on electrified interfaces, essences of DFT-MPB models and basic equations are described. Equations are derived on several significant thermodynamic and kinetic properties of electrode reactions, such as electrosorption valency value and transfer coefficient, and by the derivations, free energies and charge transfer properties are shown to be described in a self-consistent manner on the basis of the grand-canonical DFT formalism in the DFT-MPB method. Results of applications to a Pt(111) single crystal electrode are presented on surface phase diagrams, electrosorption valency values, activation free energies, transfer coefficients, IR-absorption spectroscopy and X-ray absorption spectroscopy, and by the results, the DFT-MPB is shown to be able to predict the thermodynamic, kinetic and spectroscopic properties within accuracies useful for materials design.

KEYWORDS Density Functional Theory, Modified Poisson-Boltzmann Theory, Electric Double Layer, Interfacial Electrochemistry

1. Introduction

Thermodynamics and kinetics of electrode reactions strongly depend on the electrode potential. Their activation free energies, for examples, are described by linear functions or quadratic functions of the electrode potential in Butler-Volmer equation⁽¹⁾ or Marcus equation,⁽²⁾ respectively, and potential changes by only several tens millivolt can cause changes by orders of magnitude in reaction rates. The effects of the electrode potential, therefore, should be included in any simulations of electrode reactions.

The electrode potential U scaled with the standard hydrogen electrode (SHE) is related to the electrochemical potential (or Fermi energy) μ_e of electrons in the electrode by the following equation,⁽³⁻⁵⁾

$$U = -\frac{\mu_e - \mu_e^{\text{SHE}}}{e}, \dots \dots \dots (1)$$

where μ_e^{SHE} corresponds to the electrochemical potential of electrons in the SHE. Since μ_e is an electronic property, its rigorous definition can be obtained only by electronic structure theories.

Density functional theory (DFT)⁽⁶⁻¹⁰⁾ is one of the most widespread electronic structure theories, but its applications to electrode reactions have been limited because of difficulties in descriptions of the electric double layer formed at electrolyte-electrode interfaces.

The electric double layer is a region where a polarization of the charge distribution is formed across the electrolyte-electrode interface.⁽³⁻⁵⁾ This polarization is formed to adjust μ_e in the electrode to that in the external circuit in contact with the electrode. As schematically shown in **Fig. 1(A)**, when the electrochemical potential of electrons in the external circuit is lowered from a potential of zero charge (PZC) of the electrode, for example, a positive charge is induced on the electrode surface by electron transfer from the electrode to the external circuit, and a negative charge is accumulated in the electrolyte near the electrode by anion transfer from the bulk electrolyte to the interfacial region and cation transfer from the interfacial region to the bulk electrolyte. The interfacial polarization generates an electrostatic potential gap $\Delta\phi$ across the interface, and by this polarization, μ_e in the electrode is lowered and equalized with that in the external circuit. The electric double layer is, therefore, inextricably linked to the

electrode potential and must be included into simulation models.

Big challenges of describing the double layer formation arise from its spatial and time scales. Spatially, the charge distribution in the double layer is approximately proportional to $\exp(-\kappa z)$ in a low concentration condition,^(11,12) where κ is the inverse of the Debye length, and z is the distance from the electrode surface. By this exponential function, a screening length of the induced surface charge by the double layer is roughly estimated to be 3 to 30 nm for the electrolyte with an ionic concentration of 1 to 10^{-3} mol·L⁻¹. With regard to the time scale, the relaxation time of the double layer can be approximately obtained by a Debye relaxation time,⁽¹³⁾ which is estimated as 0.05 to 50 ns for a typical aqueous electrolyte with an ionic concentration of 1 to 10^{-3} mol·L⁻¹. These estimated length- and time-scales are beyond capabilities of conventional DFT simulations, which can handle motions of only hundreds to thousands of atoms in a volume of $3 \times 3 \times 3$ nm³ during tens of pico-seconds even when a state-of-the-art peta-flops computing system is used. Approximations are, therefore, necessary.

Since the pioneering works using simple jellium models for extended surfaces or metal cluster models done in 1980s, many approximated double layer models based on electronic structure theories have

been suggested,⁽¹⁴⁾ but models applicable to practical simulations have been developed only recently. Lozovoi and Alavi⁽¹⁵⁾ approximated ion charges in the electric double layer as a simple Gaussian charge sheet, which completely screens electrostatic field formed by a charged slab as shown in Fig. 1(B). Otani and Sugino⁽¹⁶⁾ suggested a Green function technique called effective screening medium (ESM), in which the Gaussian charge sheet in Lozovoi's model is replaced by image charges induced in a perfect conductor medium placed above the charged slab as shown in Fig. 1(C) or 1-dimensional ion charge distribution obtained by solving a modified Poisson-Boltzmann (MPB) theory^(17,18) numerically as shown in Fig. 1(D). Jinnouchi and Anderson^(19,20) combined the latter model with a polarizable continuum model (PCM)^(21,22) to describe 3-dimensional ion-distribution and mean field of solvation in the electrolyte as shown in Fig. 1(E). This model is called DFT-MPB model.

Recently, our group has implemented the DFT-MPB method into a parallel DFT code and applied it to various electrode reactions in fuel cells. In this article, after an introduction of the DFT-MPB method, results of applications are presented.

2. DFT-MPB Method

2.1 Model

In the DFT-MPB model, as shown in Fig. 1(E), the electrolyte-electrode interfacial system is divided into an interfacial region comprised of the electrode surface and adsorbates (region (i)), and an outer region (region (ii)). Two well-known approximations are applied to describe the free energy of the entire electric double layer: the Born-Oppenheimer approximation⁽²³⁾ and static solvation approximation⁽²⁴⁾: the Born-Oppenheimer approximation has been applied successfully to describe electronic and nuclear motions separately by DFT⁽⁷⁻¹⁰⁾ or ab initio wave function-based methods⁽²⁵⁾; the static solvation approximation has been also applied successfully to describe the mean field of solvation by self-consistent reaction field (SCRF) methods using continuum solvation models^(19-22,26-27) or explicit atom models.^(28,29)

Atomic nuclei in the region (i) are described as mass points, and the electrons in the region (i) are described by a probability distribution corresponding to the electron density. The electron density is assumed to converge instantaneously to that at a ground state

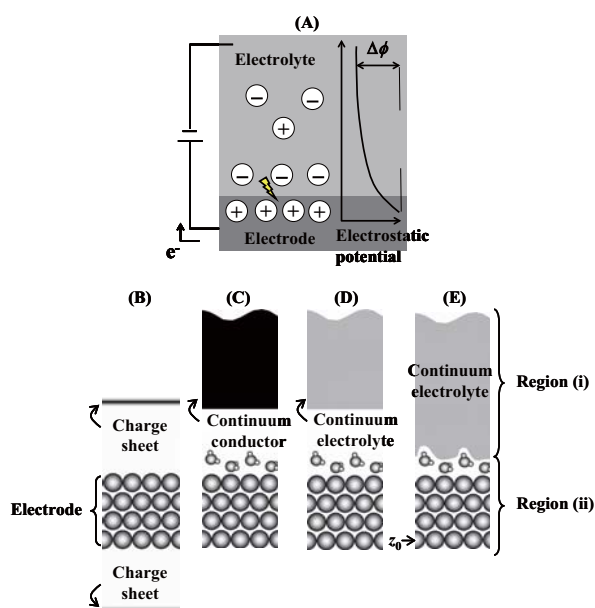


Fig. 1 Schematics of an electrolyte/electrode interface (A) and its models (B to E).

at fixed nuclear positions on the basis of the Born-Oppenheimer approximation. Since the number of electrons vary to adjust their electrochemical potential to that in an external circuit as described in the previous section, the ground state electronic structure is described by a grand-canonical DFT formalism,^(8,15,30) in which the ground state electron density is determined to minimize a ground-potential.

Similarly to the electrons, ions and solvent molecules in the region (ii) surrounding the fixed nuclei in the region (i) are described by density distribution functions on the basis of a static solvation approximation. Since the numbers of ions and solvent molecules vary also to adjust their electrochemical potentials to those in the bulk electrolyte, the distribution functions are determined to minimize a grand-potential described by a grand-canonical formalism.

2.2 Free Energy

The Hamiltonian of the nuclear motions in the region (i) is described as follows:

$$H(\mathbf{P}_i, \mathbf{R}_i) = \sum_i \frac{|\mathbf{P}_i|^2}{2M_i} + \Omega(\mathbf{R}_i) \quad , \dots \dots \dots (2)$$

where H is the Hamiltonian, \mathbf{P}_i and \mathbf{R}_i are the momentum and positions of i -th nucleus, respectively, and Ω is the grand-potential. According to a description by Lozovoi et al.,⁽¹⁵⁾ Ω is described as follows:

$$\Omega(\mathbf{R}_i) = F(\mathbf{R}_i) - \mu_e N_e(\mathbf{R}_i) - \mu_+ N_+(\mathbf{R}_i) - \mu_- N_-(\mathbf{R}_i) \quad , \dots \dots \dots (3)$$

where F is the Helmholtz free energy, μ_+ and μ_- are the electrochemical potentials of cation and anion, respectively, and N_e , N_+ and N_- are the numbers of electrons, cations and anions, respectively. As described later, the solvent molecules are described implicitly in this study, and therefore, their contributions do not appear explicitly in this equation. Similarly to the description by Lozovoi et al.,⁽¹⁵⁾ the term, ‘‘Helmholtz free energy’’, indicates the free energy with respect to subsystems of the electrons and electrolyte characterized by a certain electronic temperature T_e and an electrolyte temperature T . The term is, however, just the total energy for the nuclear

system.

By using the Hamiltonian, the Gibbs free energy G of the system is described as follows:

$$G = -k_B T \ln \int \prod_i d\mathbf{R}_i \prod_i d\mathbf{P}_i dV \exp\left(-\frac{H(\mathbf{P}_i, \mathbf{R}_i) + pV}{k_B T}\right) \quad , \dots \dots \dots (4)$$

where p is the pressure, V is the volume, and k_B is the Boltzmann constant.

Although the phase space integration in this equation can be executed numerically using a molecular dynamics method under a constant electrode potential condition,⁽³¹⁾ quantitative results are still very difficult to obtain on the interfacial electron transfer reactions. Alternatively, analytical integrations using simple statistical models^(24,32) for the nuclear motions are employed in our calculations. By this approximation, Eq. (4) is rewritten as follows:

$$G \cong \Omega(\mathbf{R}_i^0) + H_n - TS_n \quad , \dots \dots \dots (5)$$

where \mathbf{R}_i^0 is the equilibrium position of i -th nucleus, T is the nuclear temperature, and H_n and S_n are the enthalpy and entropy of the nuclear motions, respectively.

2.3 Helmholtz Free Energy of Electronic and Electrolyte Subsystems

The Helmholtz free energy functional F is described using a DFT-MPB method, in which the electrons in the region (i) are regarded as independent-particles in a one-electron effective potential, and their density is described by DFT, while the electrolyte in the region (ii) is regarded as continuum ionic distributions in a dielectric medium, and their distribution functions are described by a modified Poisson-Boltzmann (MPB) theory.^(17,18) Similarly to other self-consistent reaction field (SCRf) approaches,^(21,22,26,27) the two regions are connected with an adaptive dielectric model function.⁽¹⁹⁾

The functional F is described by a following equation:

$$F = K + E_{xc} + E_{es} + F_{ss,nes} + F_{is,nes} - T_e S_e - TS_{\pm} \quad , \dots \dots \dots (6)$$

where K is the kinetic energy of electrons, E_{xc} is the

exchange-correlation energy of the electrons, E_{es} is the electrostatic energy, $F_{ss,nes}$ is the free energy of the non-electrostatic interactions between the atoms in the region (i) and the water molecules in the region (ii), $F_{is,nes}$ is the free energy of the non-electrostatic interactions between the atoms in the region (i) and the ions in the region (ii), and S_e and S_{\pm} are entropies of the electrons and electrolyte, respectively.

Similarly to the conventional DFT formalism,⁽⁶⁻¹⁰⁾ K , E_{xc} , E_{es} and S_e in Eq. (6) are described as follows:

$$K = \sum_n \sum_{\mathbf{k}} \sum_{\sigma} f_{nk\sigma} \int d\mathbf{r} \psi_{nk\sigma}^*(\mathbf{r}) \left(-\frac{1}{2} \nabla^2 \right) \psi_{nk\sigma}(\mathbf{r}) \quad \dots \dots \dots (7)$$

$$E_{xc} = \int d\mathbf{r} f_{xc}(\rho_{\uparrow}, \rho_{\downarrow}, \nabla\rho_{\uparrow}, \nabla\rho_{\downarrow}) \quad \dots \dots \dots (8)$$

$$E_{es} = \int d\mathbf{r} [\rho_e(\mathbf{r}) + \rho_c(\mathbf{r}) + \rho_+(\mathbf{r}) + \rho_-(\mathbf{r})] \phi(\mathbf{r}) - \int d\mathbf{r} \frac{\varepsilon(\mathbf{r})}{8\pi} |\nabla\phi(\mathbf{r})|^2 \quad \dots \dots \dots (9)$$

$$S_e = \frac{1}{2\sqrt{\pi}} \sum_n \sum_{\mathbf{k}} \sum_{\sigma} \exp \left[- \left(\frac{\varepsilon_{nk\sigma} - \mu_e}{k_B T_e} \right)^2 \right] \quad \dots \dots (10)$$

where $\psi_{nk\sigma}$ is the wave function specified by n th-band index, point \mathbf{k} in the Brillouin zone and σ spin state, $f_{nk\sigma}$ and $\varepsilon_{nk\sigma}$ are its occupation number and eigenenergy, respectively, ρ_{σ} ($\sigma = \uparrow$ or \downarrow) is the density of electrons with spin index σ , ρ_e is the total electron density, ρ_c is the nuclear charge, ρ_+ and ρ_- are cation and anion densities, respectively, ϕ is the electrostatic potential, and k_B is the Boltzmann constant. For describing S_e , a Gaussian smearing method suggested by Fu and Ho⁽³³⁾ is used.

ρ_{σ} and ρ_e are related to $\psi_{nk\sigma}$ and $f_{nk\sigma}$ as follows:

$$\rho_{\sigma}(\mathbf{r}) = \sum_n \sum_{\mathbf{k}} f_{nk\sigma} |\psi_{nk\sigma}(\mathbf{r})|^2 \quad \dots \dots \dots (11)$$

$$\rho_e(\mathbf{r}) = \sum_{\sigma} \rho_{\sigma}(\mathbf{r}) \quad \dots \dots \dots (12)$$

As in usual DFT formalism, $\psi_{nk\sigma}$ and $f_{nk\sigma}$ must satisfy the following constraints:

$$\int \psi_{nk\sigma}^*(\mathbf{r}) \psi_{mk\sigma}(\mathbf{r}) d\mathbf{r} = \delta_{nm} \quad \dots \dots \dots (13)$$

$$\sum_n \sum_{\mathbf{k}} \sum_{\sigma} f_{nk\sigma} = N_e \quad \dots \dots \dots (14)$$

Unlike the conventional DFT model, the dielectric permittivity ε in Eq. (9) is a position-dependent function described as follows:

$$\varepsilon(\mathbf{r}) = 1 + \frac{\varepsilon_{\infty}(\mathbf{r}) - 1}{2} \left(1 + \frac{1 - (\rho_{na}(\mathbf{r})/\rho_0)^{2\beta}}{1 + (\rho_{na}(\mathbf{r})/\rho_0)^{2\beta}} \right) \quad \dots \dots \dots (15)$$

where ρ_0 and β are constant parameters and are set as 0.00057 bohr⁻³ and 1.3, respectively, according to the recommendation in the literatures,^(19,21,22) and ρ_{na} is a summation of ground-state electron densities of neutral atoms.⁽¹⁹⁾ In the region far from nuclear positions in the region (i), ε approaches ε_{∞} , which is defined as the following function:

$$\varepsilon_{\infty}(\mathbf{r}) = \begin{cases} \frac{\varepsilon_b - 1}{2} \left(1 - \operatorname{erf} \left(\frac{z - z_0}{\Delta z} \right) \right) + \varepsilon_b, & \text{for surface system} \\ \varepsilon_b, & \text{for system other than surface} \end{cases} \quad \dots \dots \dots (16)$$

where ε_b is the dielectric permittivity of the bulk electrolyte, z_0 is the position of the bottom of the slab, z is the distance from z_0 , and Δz is a constant parameter and set as 1 Å. Details of the physical background of the equations and parameters are described in Ref. 19.

The non-electrostatic free energy $F_{ss,nes}$ in Eq. (6) is a summation of cavitation, dispersion and repulsion free energies, which are denoted as $F_{ss,cav}$, $F_{ss,dr}$ and $F_{ss,rep}$, respectively. The cavitation free energy $F_{ss,cav}$ is described as a product of a total surface area A of the atoms in the region (i) and a surface tension γ_b of the bulk electrolyte as follows:

$$F_{ss,cav} = \gamma_b A \quad \dots \dots \dots (17)$$

The dispersion and repulsion free energies are obtained each as a linear function of atomic surface areas A_i as follows:

$$F_{ss,dr} = \sum_i (a_i^{dr} A_i + b_i^{dr}) \quad \dots \dots \dots (18)$$

$$F_{ss,rep} = \sum_i (a_i^{rep} A_i + b_i^{rep}) \quad \dots \quad (19)$$

Details of the methods to obtain the total and atomic surface areas A and A_i are described in Ref. 19.

The non-electrostatic interaction energy $F_{is,nes}$ is described as follows:

$$F_{is,nes} = \int d\mathbf{r} (|\rho_-(\mathbf{r})| + |\rho_+(\mathbf{r})|) \phi_{rep}(\mathbf{r}) \quad \dots \quad (20)$$

where ϕ_{rep} represents non-electrostatic repulsive potentials between atoms in the region (i) and ions in the region (ii). The repulsive interaction prevents ions in the region (ii) from approaching atoms in the region (i) too closely. A similar repulsive potential was introduced by Otani and Sugino⁽¹⁶⁾ for describing a Stern layer, and the methodology was modified in an adaptive manner by Jinnouchi and Anderson.⁽¹⁹⁾

The entropy S_{\pm} is described using a lattice gas model as follows:

$$S_{\pm} = -\frac{k_B}{a^3} \int d\mathbf{r} [|\rho_+(\mathbf{r})| a^3 \ln(|\rho_+(\mathbf{r})| a^3) + |\rho_-(\mathbf{r})| a^3 \ln(|\rho_-(\mathbf{r})| a^3) + (1 - |\rho_+(\mathbf{r})| a^3 - |\rho_-(\mathbf{r})| a^3) \ln(1 - |\rho_+(\mathbf{r})| a^3 - |\rho_-(\mathbf{r})| a^3)] \quad \dots \quad (21)$$

This term was introduced by Borukhov et al.^(17,18) to describe steric effects of ion in solution.

2.4 Minimization of Grand-potential

Ω is a functional of $\psi_{nk\sigma}, f_{nk\sigma}, \rho_{\pm}$ and ϕ , and can be minimized by simultaneously solving equations obtained by variational principles:

$$\left[-\frac{1}{2} \nabla^2 + \frac{\delta E_{xc}}{\delta \rho_e} + \phi(\mathbf{r}) \right] \psi_{nk\sigma}(\mathbf{r}) = \varepsilon_{nk\sigma} \psi_{nk\sigma}(\mathbf{r}) \quad \dots \quad (22)$$

$$\nabla \cdot (\varepsilon(\mathbf{r}) \nabla \phi(\mathbf{r})) = -4\pi (\rho_e(\mathbf{r}) + \rho_c(\mathbf{r}) + \rho_+(\mathbf{r}) + \rho_-(\mathbf{r})) \quad \dots \quad (23)$$

$$\rho_{\pm}(\mathbf{r}) = \mp \frac{c_b e^{(\pm\phi(\mathbf{r}) - \phi_{rep}(\mathbf{r})) / k_B T}}{1 - 2a^3 c_b + 2a^3 c_b \cosh(\phi(\mathbf{r}) / k_B T) e^{-\phi_{rep}(\mathbf{r}) / k_B T}} \quad \dots \quad (24)$$

$$T_e \frac{\partial S_e}{\partial f_{nk\sigma}} = \varepsilon_{nk\sigma} - \mu_e \quad \dots \quad (25)$$

Ω depends also on nuclear positions \mathbf{R}_i and can be minimized by conventional quasi-Newton methods⁽³⁴⁾ using the following analytical derivatives of Ω with respect to \mathbf{R}_i :

$$\nabla_{\mathbf{R}_i} \Omega = -\mathbf{F}_{HF} - \mathbf{F}_{Pulay} - \mathbf{F}_{solv,nes} \quad \dots \quad (26)$$

$$\mathbf{F}_{HF} = -\int d\mathbf{r} \nabla_{\mathbf{R}_i} \rho_c(\mathbf{r}) \phi(\mathbf{r}) \quad \dots \quad (27)$$

$$\mathbf{F}_{Pulay} = -\sum_{\sigma} \sum_{\mathbf{k}} \sum_n f_{nk\sigma} \int d\mathbf{r} [\nabla_{\mathbf{R}_i} \psi_{nk\sigma}^*(\mathbf{r}) (\hat{H} - \varepsilon_{nk\sigma}) \psi_{nk\sigma}(\mathbf{r}) + \psi_{nk\sigma}^*(\mathbf{r}) (\hat{H} - \varepsilon_{nk\sigma}) \nabla_{\mathbf{R}_i} \psi_{nk\sigma}(\mathbf{r})] \quad \dots \quad (28)$$

$$\mathbf{F}_{solv,nes} = \frac{1}{8\pi} \int d\mathbf{r} \nabla_{\mathbf{R}_i} \rho_{na}(\mathbf{r}) \frac{d\varepsilon}{d\rho_{na}} |\nabla \phi(\mathbf{r})|^2 - \int d\mathbf{r} \nabla_{\mathbf{R}_i} \rho_{na}(\mathbf{r}) \frac{\delta F_{ss,nes}}{\delta \rho_{na}} - \int d\mathbf{r} (|\rho_-(\mathbf{r})| + |\rho_+(\mathbf{r})|) \nabla_{\mathbf{R}_i} \phi_{rep}(\mathbf{r}) \quad \dots \quad (29)$$

For efficient computations using pseudopotentials and projector expansions, the grand-potential and its derivatives must be reorganized. Details of these reorganizations are shown in Ref. 19.

2.5 Numerical Procedure for Minimization

A flowchart of the numerical procedure to minimize Ω is shown in **Fig. 2**. A major difference between the DFT-MPB calculations and conventional DFT calculations is in their calculations of the electrostatic potential ϕ . In the conventional DFT calculations on molecules and surfaces in vacuum, ϕ is obtained by solving the following Poisson equation:

$$\nabla^2 \phi(\mathbf{r}) = -4\pi [\rho_e(\mathbf{r}) + \rho_c(\mathbf{r})] \quad \dots \quad (30)$$

which is obtained by substituting $\varepsilon = 1$ and $\rho_{\pm} = 0$ into Eq. (23). This Poisson equation can be solved by conventional reciprocal- or real-space numerical

methods.⁽³⁵⁻³⁷⁾ In the case of the DFT-MPB calculations, ϕ is obtained by solving the modified Poisson-Boltzmann equations (23) and (24), and in our implementation,⁽¹⁹⁾ the equations are iteratively solved by a real-space method using a point-successive over relaxation (PSOR) method⁽³⁸⁾ combined with a multi-grid method,⁽³⁹⁾ which was shown to be efficient for calculations not only on molecular systems but also on surface systems.

In the DFT-MPB method, additional computations are necessary also to obtain free energy terms E_{es} , $F_{ss,nes}$, $F_{is,nes}$ and S_{\pm} and their derivatives with respect to \mathbf{R}_i . These calculations can be easily executed by using real-space quadrature schemes.^(36,37,40,41)

3. Properties Calculated from DFT-MPB: Thermodynamics, Kinetics and Spectroscopy

By using the DFT-MPB method, valuable information is obtained on thermodynamics and kinetics of electrode reactions, and spectroscopic properties of reaction intermediates. In this section,

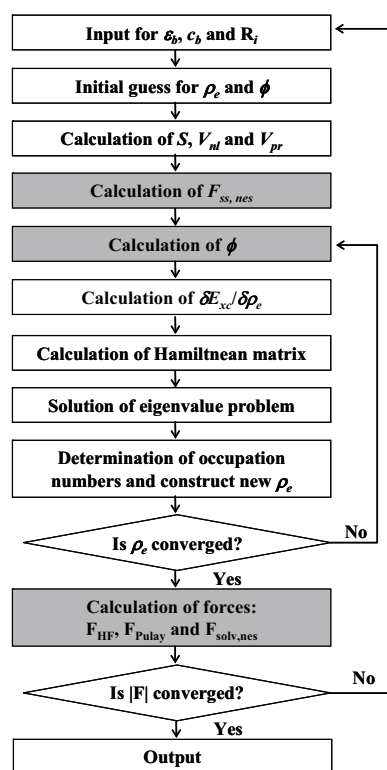


Fig. 2 Flowchart of DFT-MPB calculations. Differences from conventional DFT calculations are in the steps shown as gray squares.

results of applications are presented after brief introductions of the calculation methods.

3. 1 Reaction Free Energies and Reversible Potentials

3. 1. 1 Method

Reaction free energies and redox potentials are important thermodynamic properties to predict phase stabilities of electrode surfaces. In the DFT-MPB method, the thermodynamic properties are obtained by calculating the Gibbs free energy G_I described as Eq. (5) and the electrode potential U_I described as Eq. (1) changing the number $N_{e,I}$ of electrons present in the system. Here, the subscript I denotes the product state P or reactant state R. As shown in **Fig. 3** (A), obtained discrete data G_I and U_I are interpolated by a quadratic function as follows:

$$G_I \cong a_I U^2 + b_I U + c_I, \quad (I = \text{R or P}), \dots \dots (31)$$

and the reaction free energy ΔG is obtained as a difference between the quadratic function of a reactant and that of its product. The redox potential for forming the product P from the reactant R is obtained as a crossing point between the two quadratic curves.

3. 1. 2 Results on Surface Phase Diagrams of Pt(111)

Figure 4 (A) shows calculated reaction free energies of the following H, OH and O adsorbate formations on Pt(111):^(20,43-48)

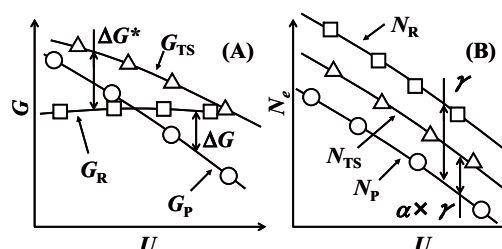


Fig. 3 $G-U$ (A) and N_e-U (B) plots. From differences in the interpolated curves, various properties are obtained on reaction free energy ΔG , activation free energy ΔG^* , electroadsorption valency value γ and transfer coefficient α .

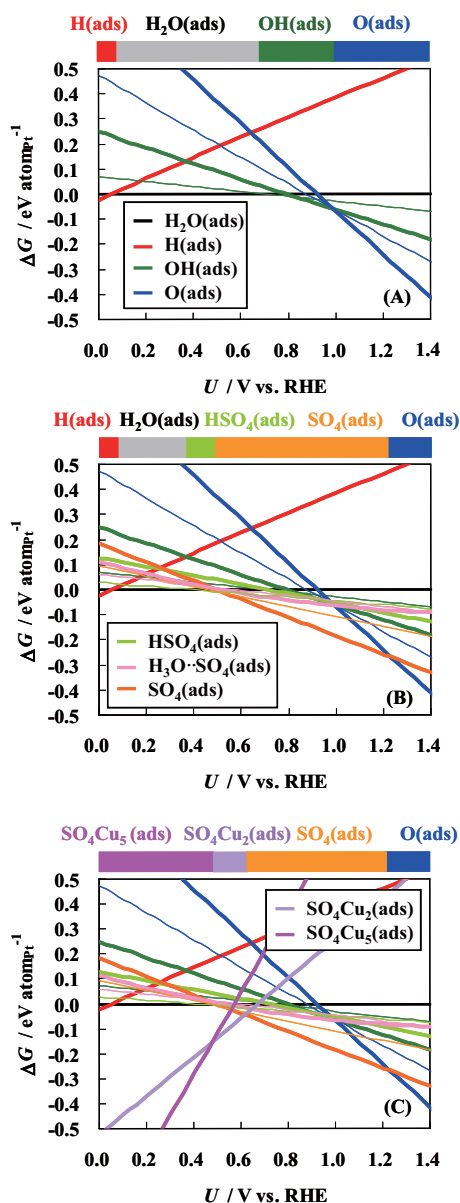
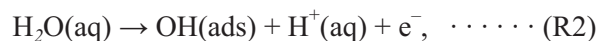


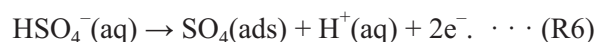
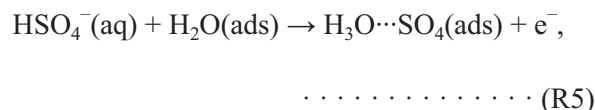
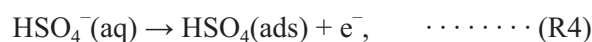
Fig. 4 Reaction free energies ΔG for reactions (R1) – (R8) as functions of electrode potential U . Thinner lines are the results under low surface coverage conditions (1/12 ML for OH(ads), 1/4 ML for O(ads), 1/10 ML for bisulfate (HSO₄(ads)), hydronium-sulfate ion pair (H₃O⁺·SO₄(ads)) and sulfate (SO₄(ads)), and thicker lines are the results under high surface coverage conditions (1/3 ML for H(ads), 1/3 ML for OH(ads), 1/2 ML for O(ads), 1/5 ML for bisulfate (HSO₄(ads)), hydronium-sulfate ion pair (H₃O⁺·SO₄(ads)) and sulfate (SO₄(ads)), and 2/3 ML for deposited Cu (SO₄Cu₂(ads)), and 1 ML for deposited Cu (SO₄Cu₅(ads)). Bars above graphs indicate stable phases deduced from the reaction free energies. Electrolytes considered in these calculations are 0.1M HClO₄ for (A), 0.1M H₂SO₄ for (B) and 0.1M H₂SO₄+5 mM CuSO₄ for (C).



where (aq) and (ads) indicate the aqueous phase and adsorbate phase, respectively. The results indicate that H(ads), OH(ads) and O(ads) are stable in the potential ranges of $U \leq 0.11$ V, $0.69 < U \leq 0.99$ V and $0.99 < U$, respectively. The theoretical results are consistent with the experimentally-obtained cyclic voltammograms of Pt(111) in a HClO₄ solution,^(49,50) from which H(ads), OH(ads) and O(ads) are judged to be stable in the potential range of $U \leq 0.24$ V, $0.73 < U \leq 0.98$ V and $0.98 < U$, respectively.

The OH and O adsorbate formation reactions (R2) and (R3) are known to be disturbed by specifically adsorbed sulfuric acid anion when the HClO₄ solution is replaced by a H₂SO₄ solution.^(51,52) This specific adsorption also can be described well by the DFT-MPB method.⁽⁵³⁾

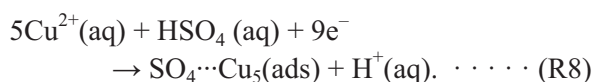
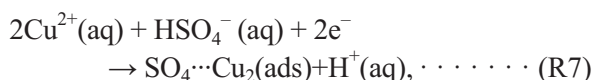
Figure 4(B) shows reaction free energies for the following anion adsorption reactions in addition to those for reactions (R1) – (R3):



Bisulfate with the surface coverage θ_s of 1/10 ML is stable in $0.41 < U \leq 0.48$ V, but within the narrow free energy range of about $-0.01 < \Delta G \leq 0.02$ eV, there are three other surface states: sulfate with $\theta_s = 1/10$ ML, hydronium-sulfate ion pair with $\theta_s = 1/10$ ML and 1/5 ML. In the higher potential range of $0.48 < U$, sulfate with $\theta_s = 1/10$ and 1/5 ML is stable. This means that when the electrode potential is increased from a low potential [e.g., $U = 0.20$ V] in the presence of sulfuric acid, anion adsorption starts at $U \approx 0.4$ V. At the initial stage of the adsorption, bisulfate is the main adsorbate, but sulfate and hydronium-sulfate ion pair can also coadsorb due to the small free energy differences. As the potential becomes higher, bisulfate and hydronium-sulfate ion pair gradually disappear and sulfate becomes the main adsorbate. Because the free energy of sulfate is lower than those of OH(ads) and O(ads), sulfate suppresses hydroxide adsorption

and oxide formation. Sulfate is, therefore, judged to be stable in a wide potential range.

When copper cation (Cu^{2+}) is introduced into the H_2SO_4 solution, cation is deposited on the surface and forms sub-monolayer of Cu layer co-adsorbed with sulfate at the potential higher than the bulk deposition potential of Cu (0.34 V (SHE)).^(54,55) This so-called underpotential deposition of Cu (Cu-UPD) is also described well by the DFT-MPB method.⁽⁵⁶⁾ Figure 4(C) shows reaction free energies for the following deposition reactions in addition to those for reactions (R1) – (R6):



2/3 ML of copper co-adsorbed with 1/3 ML of sulfate formed by the reaction (R7) is stable at $0.49 < U \leq 0.63$ V (RHE), and 1 ML of copper co-adsorbed with 1/5 ML of sulfate formed by the reaction (R8) is stable at $0.34 < U \leq 0.49$ V (RHE). The results indicate that when the electrode potential is decreased from a high potential [e.g., $U = 0.80$ V] in the presence of copper cation, Cu-UPD proceeds by two-step mechanism: the formation of 2/3 ML of copper at $U = 0.63$ V (RHE) followed by the formation of 1 ML of copper at 0.49 V (RHE). The results are consistent with the experimentally-obtained linear sweep voltammograms,⁽⁵⁵⁾ in which two sharp current spikes attributed to the copper depositions are observed at $U = 0.65$ V and 0.61 V (RHE).

Table 1 summarizes the reversible potentials forming adlayers which appear in the reactions (R1) – (R8). The theoretically-obtained reversible potentials agree well with the experimentally-obtained ones. The results indicate that thermodynamics of the electrode reactions are accurately described by the DFT-MPB method.

3. 2 Electrosorption Valency Values

3. 2. 1 Method

Electrosorption valency value γ is an essential electrochemical property related to thermodynamics and charge transfer properties of electrode reactions. γ is defined as the number of charges transferred by an

adsorbate formation and is described as the following equation:

$$\gamma = - \frac{1}{e} \frac{\partial \sigma_{\text{surf}}}{\partial \theta} \Big|_{T,p,U}, \dots \dots \dots (32)$$

where σ_{surf} is the surface charge density, and θ is the surface coverage of the adsorbate.^(4,5,52,57) Another important description of γ is obtained by cross differentiations of an electrocapillary equation as follows:^(4,5,53,57)

$$\gamma = \frac{1}{e} \frac{\partial \Delta G}{\partial U} \Big|_{T,p,\theta}, \dots \dots \dots (33)$$

In the conventional DFT calculations on non-electrified interfaces, the surface charge σ_{surf} is empirically determined to neutralize the surfaces. In other words, γ cannot be obtained by the theory. In contrast, the

Table 1 Reversible potentials U_{rev} (V vs. RHE) for reactions (R1) – (R8). Experimental values were obtained from cyclic voltammograms reported in the literatures.

Reaction	U_{rev} (Cal.)	U_{rev} (Exp.)
$\text{H}^+(\text{aq}) + \text{e}^- \leftrightarrow \text{H}(\text{ads})$	0.11	0.24 ^a
$\text{H}_2\text{O}(\text{aq}) \leftrightarrow \text{OH}(\text{ads}) + \text{H}^+(\text{aq}) + \text{e}^-$	0.69	0.73 ^a
$\text{OH}(\text{ads}) \leftrightarrow \text{O}(\text{ads}) + \text{H}^+(\text{aq}) + \text{e}^-$	0.99	0.98 ^b
$\text{HSO}_4^-(\text{aq}) \leftrightarrow \text{HSO}_4(\text{ads}) + \text{e}^-$	0.41	0.44 ^c
$\text{HSO}_4^-(\text{aq}) \leftrightarrow \text{H}_3\text{O} \cdots \text{SO}_4(\text{ads}) + \text{e}^-$	0.55	–
$\text{HSO}_4(\text{ads}) \leftrightarrow \text{SO}_4(\text{ads}) + \text{H}^+(\text{aq}) + \text{e}^-$	0.46	-0.5 ^d
$3\text{SO}_4(\text{ads}) + 10\text{Cu}^{2+}(\text{aq}) + 2\text{HSO}_4^-(\text{aq}) + 16 \text{e}^- \leftrightarrow 5(\text{SO}_4 \cdots \text{Cu}_2)(\text{ads}) + 2\text{H}^+(\text{aq})$	0.63	0.65 ^e
$5(\text{SO}_4 \cdots \text{Cu}_2)(\text{ads}) + 5\text{Cu}^{2+}(\text{aq}) + 2\text{H}^+(\text{aq}) + 14 \text{e}^- \leftrightarrow 3(\text{SO}_4 \cdots \text{Cu}_5)(\text{ads}) + 2\text{HSO}_4^-(\text{aq})$	0.49	0.61 ^e

- Potentials forming 1/3 ML of H(ads) and 1/12 ML of OH(ads) reported in Ref. 49. Contributions from configurational entropies $k_B T \ln [\theta / (1 - \theta)]$ were subtracted.
- Potential estimated from a scan rate dependence of the cyclic voltammogram reported in Ref. 50.
- Potential forming 1/10 ML of bisulfate adlayer reported in Ref. 52.
- A potential, where a transient in the electrosorption valency value appears, reported in Ref. 52.
- Potentials reported in Ref. 54.

DFT-MPB method can handle explicitly the electrified interfaces, and γ can be theoretically obtained in a self-consistent manner.

An equation to obtain γ by the DFT-MPB method is derived as follows. By using a thermodynamic integration scheme,⁽⁵⁸⁾ the reaction free energy ΔG is described as follows:

$$\Delta G = \int_{\xi_R}^{\xi_P} \frac{d}{d\xi} \left[-k_B T \ln \int \exp \left[-\frac{H(\mathbf{P}_i, \mathbf{R}_i) + pV}{k_B T} \right] d\mathbf{P}_i \prod_{i \neq \xi} d\mathbf{P}_i d\mathbf{R}_i dV \right] d\xi, \quad \dots \dots \dots (34)$$

where ξ is the reaction coordinate, and ξ_I ($I = R$ or P) is the position of the reactant or product on the reaction coordinate. By substituting Eqs. (1), (2) and (34) into Eq. (33), the following equation is obtained:

$$\begin{aligned} \gamma &= \frac{1}{e} \left. \frac{\partial \Delta G}{\partial U} \right|_{T, p, \theta} \\ &= \frac{1}{e} \int_{\xi_R}^{\xi_P} \frac{d}{d\xi} \frac{\partial}{\partial U} \left[-k_B T \ln \int \exp \left[-\frac{1}{k_B T} \left\{ \sum_i \frac{|\mathbf{P}_i|^2}{2M_i} + \Omega(\mathbf{R}_{i \neq \xi}, \xi) + pV \right\} \right] d\mathbf{P}_i \prod_{i \neq \xi} d\mathbf{P}_i d\mathbf{R}_i dV d\xi \right. \\ &= - \int_{\xi_R}^{\xi_P} \frac{d}{d\xi} \frac{1}{Q(\xi)} \left[\int \frac{\partial \Omega}{\partial \mu_e} \exp \left[-\frac{1}{k_B T} \left\{ \sum_i \frac{|\mathbf{P}_i|^2}{2M_i} + \Omega(\mathbf{R}_{i \neq \xi}, \xi) + pV \right\} \right] d\mathbf{P}_i \prod_{i \neq \xi} d\mathbf{P}_i d\mathbf{R}_i dV d\xi \right. \end{aligned} \quad \dots \dots \dots (35)$$

where $Q(\xi)$ is the partition function defined as follows:

$$Q(\xi) = \int \exp \left[-\frac{1}{k_B T} \left\{ \sum_i \frac{|\mathbf{P}_i|^2}{2M_i} + \Omega(\mathbf{R}_{i \neq \xi}, \xi) + pV \right\} \right] d\mathbf{P}_i \prod_{i \neq \xi} d\mathbf{P}_i d\mathbf{R}_i dV \quad (36)$$

By using Janak theorem⁽⁵⁹⁾, $\partial \Omega / \partial \mu_e$ is rewritten as follows:

$$\frac{\partial \Omega}{\partial \mu_e} = \frac{\partial N_e}{\partial \mu_e} \frac{\partial F}{\partial N_e} - N_e - \mu_e \frac{\partial N_e}{\partial \mu_e} = \mu_e \frac{\partial N_e}{\partial \mu_e} - N_e - \mu_e \frac{\partial N_e}{\partial \mu_e} = -N_e \quad \dots \dots \dots (37)$$

Substituting Eq. (37) into Eq. (35) gives the following equation:

$$\begin{aligned} \gamma &= \int_{\xi_R}^{\xi_P} \frac{d}{d\xi} \frac{1}{Q(\xi)} \left[\int N_e(\mathbf{R}_{i \neq \xi}, \xi) \exp \left[-\frac{1}{k_B T} \left\{ \sum_i \frac{|\mathbf{P}_i|^2}{2M_i} + \Omega(\mathbf{R}_{i \neq \xi}, \xi) + pV \right\} \right] d\mathbf{P}_i \prod_{i \neq \xi} d\mathbf{P}_i d\mathbf{R}_i dV \right] d\xi \\ &= \int_{\xi_R}^{\xi_P} \frac{d}{d\xi} \langle N_e \rangle_{\xi} d\xi = \langle N_e \rangle_{\xi_P} - \langle N_e \rangle_{\xi_R} \quad \dots \dots \dots (38) \end{aligned}$$

Accordingly, γ is equal to the number of electrons transferred by the reaction. The resulting equation is consistent with the macroscopic thermodynamic relationship described by Eqs. (32) and (33).

The right hand side of Eq. (38) is approximated as a difference between two quadratic curves:

$$N_{e,I} \cong s_I U^2 + t_I U + u_I, \quad (I = R \text{ or } P) \quad \dots \dots \dots (39)$$

which are obtained by interpolating discrete data $N_{e,I}$ and U_I as shown in Fig. 3 (B) after the calculations of the reaction free energies ΔG by a methodology described in Subsection 3.1.1.

3. 2. 2 Results on Electrosorption Valency Value of Sulfuric Acid Anion Adsorption

Figure 5 shows calculated γ of the sulfuric anion adsorption reactions (R4) – (R6).⁽⁵³⁾ An experimental result obtained by Kolics and Wieckowski⁽⁵²⁾ is shown

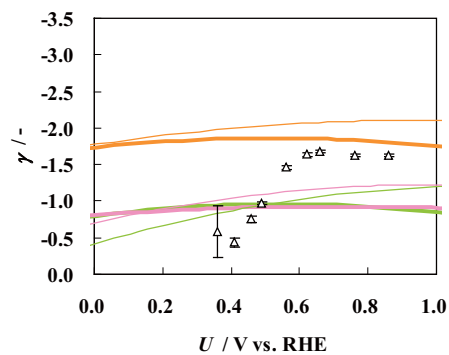


Fig. 5 Electroadsorption valency values γ for sulfuric acid anion adsorptions. Open triangles are the experimental result reported in Ref. 52. Similarly to Fig. 4, thinner lines are the results under the low surface coverage conditions. Electrolyte considered in this calculation is 0.1M H₂SO₄.

also in this figure. γ is from -0.4 to -1.2 for bisulfate and hydronium-sulfate ion pair, while it is from -1.7 to -2.1 for sulfate. Since the dominant adsorbed anion is bisulfate in $0.41 < U \leq 0.48$ V and sulfate in $0.48 \text{ V} < U$ as described in subsection 3.1.2, γ is predicted to be from -0.45 to -0.95 at $0.41 < U \leq 0.48$ V and from -1.75 to -1.85 at $U > 0.48$ V. The calculated values are in good agreement with the experiment (from -0.6 to -1.2 in $0.35 < U \leq 0.50$ V (RHE) and from -1.5 to -1.8 in $0.55 < U \leq 0.85$ V (RHE)).

This good agreement indicates that the potential-dependent interfacial charge distribution is described correctly by the DFT-MPB method. The agreement also supports the conclusion obtained theoretically on the mechanism of the specific adsorption of anion described in subsection 3.1.2.

3.3 Activation Free Energy

3.3.1 Method

In the DFT-MPB method, the activation free energy ΔG^* is calculated by a methodology similar to that used for the calculation of the reaction free energy ΔG described in section 3.1.1. In the calculation of ΔG^* , saddle points on the grand-potential Ω are determined changing the number of electrons $N_{e,TS}$, and free energies G_{TS} at the saddle points are computed by executing a phase space integral with respect to all the coordinates other than a reaction coordinate ξ by using a harmonic oscillator model⁽³²⁾ as follows:

$$G_{TS} = -k_B T \ln \int d\mathbf{P}_\xi \prod_{i \neq \xi} d\mathbf{P}_i d\mathbf{R}_i dV \exp\left(-\frac{H(\mathbf{P}_i, \mathbf{R}_i) + pV}{k_B T}\right) \\ = \Omega(\mathbf{R}_i^{TS}) + H_n^{TS} - TS_n^{TS} \quad \dots \dots \dots (40)$$

The obtained discrete data on G_{TS} and U_{TS} are interpolated by a quadratic function:

$$G_{TS} \cong a_{TS} U^2 + b_{TS} U + c_{TS} \quad \dots \dots \dots (41)$$

and ΔG^* is obtained as $G_{TS} - G_R$ as shown in Fig. 3(A). For searching the saddle points, conventional methods, such as nudged elastic band methods^(60, 61) and dimer methods,⁽⁶²⁾ are available.

3.3.2 Results on Activation Free Energies of O and OH Formations and Reductions

Figure 6 shows potential-dependent activation free energies of O and OH formations and their reductions at a low surface coverage condition:



The activation free energies are fitted well by linear functions of the electrode potential U . The results indicate that the rates of the reactions (R9) and (R10) are described well by Butler-Volmer equations.⁽¹⁾

Parameters in the Butler-Volmer equations are, however, different between the reactions (R9) and (R10). ΔG^* at the reversible potential for the reaction (R9) is lower than that for the reaction (R10), and therefore, the exchange current density is judged to be smaller for the reaction (R10) than for the reaction (R9). The result is consistent with experimentally-obtained cyclic voltammograms, in which reduction and oxidation currents of the reaction (R9) are highly reversible,^(45, 49) while those for the reaction (R10) are irreversible.⁽⁵⁰⁾

Another distinct difference is in the transfer coefficient. In the case of the reaction (R9), the slope $|\partial \Delta G^* / \partial U|$ for the oxidative direction is close to that for the reductive direction. This result indicates that the transfer coefficient α of the reaction (R9), which is defined as $(\partial \Delta G^* / \partial U) / (e \Delta N_e)$,^(4, 5) is near-symmetric. In the case of the reaction (R10), in contrast, $|\partial \Delta G^* / \partial U|$ for the reductive direction is much larger than that for

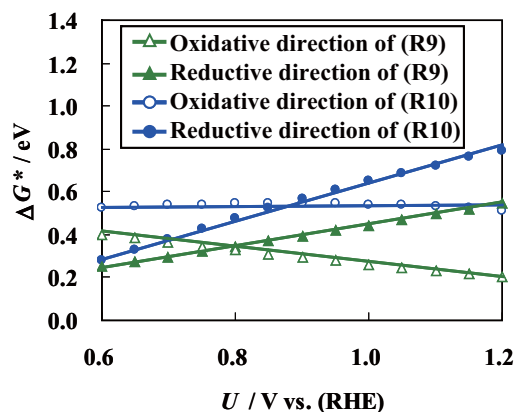


Fig. 6 Activation free energies ΔG^* for reactions (R9) and (R10) as functions of the electrode potential U .

the oxidative direction. The transfer coefficient for this reaction is, therefore, far from symmetric.

A question now arises on the origin of this difference in the transfer coefficients. An answer to the question is obtained by analyzing the number of electrons transferred by the reactions as described in the next section.

3.4 Transfer Coefficient

3.4.1 Method

As described in many textbooks,^(4,5,63) asymmetry in the transfer coefficient α has been considered to be closely related to the charge transfer properties and transition state structure. By using the thermodynamic integration scheme similarly to that used in subsection 3.2.1, an equation relating α to the charge transfer properties is obtained as follows:

$$\begin{aligned} \alpha &= \frac{1}{\Delta N_e e} \frac{d\Delta G^*}{dU} \\ &= \frac{1}{\Delta N_e e} \int_{\xi_R}^{\xi_{TS}} \frac{d}{d\xi} \frac{\partial}{\partial U} [-k_B T \\ &\quad \times \ln \int \exp[-\frac{H(\mathbf{P}_i, \mathbf{R}_i) + pV}{k_B T}] d\mathbf{P}_i \prod_{i \neq \xi} d\mathbf{P}_i d\mathbf{R}_i dV] d\xi \\ &= \frac{1}{\Delta N_e} \int_{\xi_R}^{\xi_{TS}} \frac{d}{d\xi} \langle N_e \rangle_{\xi} d\xi \\ &= \frac{\langle N_e \rangle_{\xi_{TS}} - \langle N_e \rangle_{\xi_R}}{\langle N_e \rangle_{\xi_p} - \langle N_e \rangle_{\xi_R}} \\ &= \frac{\langle N_e \rangle_{\xi_{TS}} - \langle N_e \rangle_{\xi_R}}{\gamma}, \end{aligned} \quad \dots \dots \dots (42)$$

where ΔN_e is the number of electrons transferred by the overall reaction and is equal to $\langle N_e \rangle_{\xi_p} - \langle N_e \rangle_{\xi_R}$. This equation indicates that α corresponds to the ratio of the number of electrons transferred by the formation of the transition state to ΔN_e , the number of electrons transferred by the formation of the product state.

Similarly to the case of γ , the discrete data $N_{e,TS}$ and U_{TS} , which are obtained in the calculations described in subsection 3.3.1, are interpolated by the following quadratic function:

$$N_{e,TS} \cong s_{TS} U^2 + t_{TS} U + u_{TS} \quad , \dots \dots \dots (43)$$

and α is obtained from $N_{e,TS} - N_R$ as shown in Fig. 3(B).

3.4.2 Results on Transfer Coefficients of O and OH Formations and Reductions

Figure 7 shows calculated transfer coefficients α for the reductive directions of the reactions (R9) and (R10). α for the reaction (R9) is closer to 0.5 than that for the reaction (R10). The results are consistent with the results shown in Figs. 8(A) and (B) and indicate that at the transition state, more electrons are

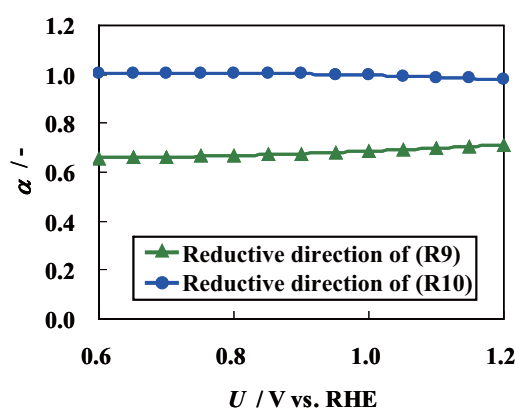


Fig. 7 Transfer coefficients α for reductive directions of reactions (R9) and (R10) as functions of the electrode potential U .

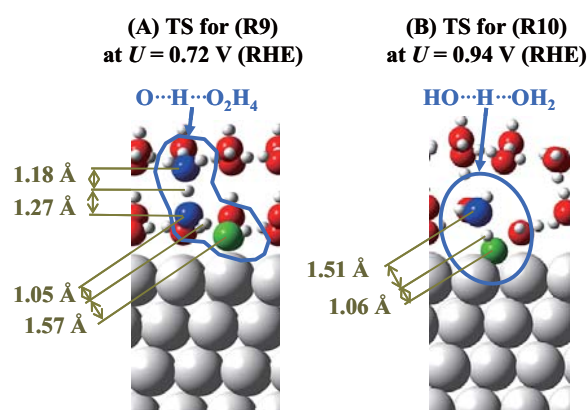


Fig. 8 Transition state structures of reactions (R9) and (R10). Small spheres are H atoms, medium spheres are O atoms, and large spheres are Pt atoms. O atoms in H_3O^+ and $H_2O_5^+$ are shown as blue spheres, and O atoms in adsorbates are shown as green spheres.

transferred by the reductive reaction (R10) than by the reductive reaction (R10).

The difference in the number of transferred electrons stems from the difference in the transition state structures. As shown in Fig. 8(B), at the transition state of the reaction (R10), a proton transferring from a hydronium ion (H_3O^+) is located closely to the adsorbed O, and the formation of adsorbed OH, which involves electron transfers, is mostly completed. In contrast, as shown in Fig. 8(A), at the transition state of the reaction (R2), a proton transferring from Zundel ion (H_5O_2^+) is far from the adsorbed OH, and therefore, the formation of H_2O is not completed.

The structural difference in the transition states between the reactions (R9) and (R10) probably stems from geometrical differences between adsorbed OH and adsorbed O. OH is adsorbed at an atop site similarly to adsorbed H_2O , and therefore, the formation of H_2O from OH proceeds through a proton hopping without large barriers involved in significant motions of oxygen atoms. In contrast, O is adsorbed at an fcc hollow site, and this oxygen atom is required to move significantly to form OH at the atop site. The motion involves a large activation barrier and cannot occur until a proton approaches the oxygen atom and pulls it up onto the atop site.

As illustrated by the results shown in this subsection, macroscopic Tafel slopes are, in fact, closely related to atomic-scale charge transfer properties and transition state structures. Obtained equations and their computational method shown in this subsection will provide new insights into atomic-scale mechanisms of elementary electrode reactions.

3.5 In situ Vibrational Spectroscopy

3.5.1 Method

Potential-dependent vibrational spectra of adsorbates at electrified interfaces give valuable information on adsorbate structures and natures of metal-adsorbate interactions in experiments.⁽⁶⁴⁾ By the DFT-MPB method, the spectra can be obtained also by solving a following eigen-equation:

$$\mathbf{H}\mathbf{x}_n = \omega_n^2 \mathbf{x}_n, \dots \dots \dots (44)$$

where \mathbf{H} is a Hessian matrix at an equilibrium point on the grand-potential Ω . Similarly to the calculations

described in previous sections, \mathbf{H} is constructed changing the number N_e of electrons, and eigenvalues ω_n and eigenvector \mathbf{x}_n are computed for each of charged states. Vibration frequencies are obtained from ω_n , vibrational modes are obtained from \mathbf{x}_n , and infrared absorption intensities are obtained from dynamic dipole moments along the vibrational modes \mathbf{x}_n .

3.5.2 Results on in situ IRAS of Sulfate Adsorbed on Pt(111)

Figure 9(A) shows calculated vibrational spectra of sulfate adsorbed on Pt(111).⁽⁵³⁾ Sulfate has a strong band at 1250 cm^{-1} and a weak band at 950 cm^{-1} . The 1250-cm^{-1} band of sulfate can be assigned to the S–O (uncoordinated) stretching mode, while the 950-cm^{-1} band presumably can be assigned to the totally symmetric S–O stretching mode. The latter mode is infrared-inactive for free sulfate ion (T_d symmetry)⁽⁶⁵⁾ but becomes active by the adsorption through the symmetry reduction to pseudo- C_{3v} . The symmetry reduction also splits the triply degenerate S–O stretching modes at 1104 cm^{-1} for free sulfate ion⁽⁶⁵⁾

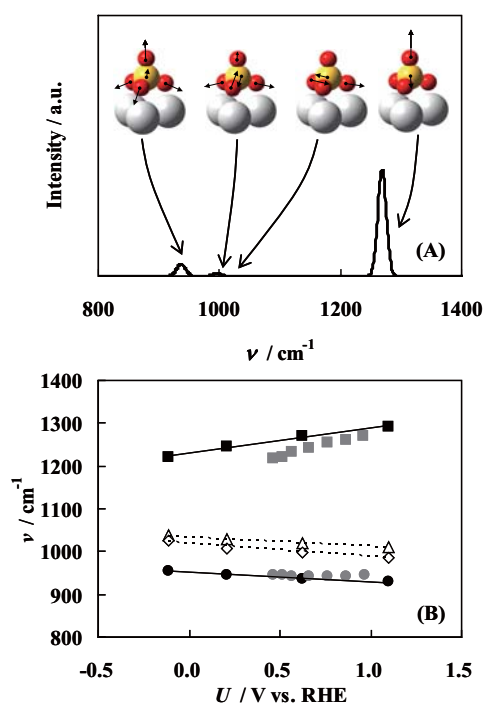


Fig. 9 Simulated IR-spectra (A) and potential-dependent vibration frequencies of sulfate adsorbed on Pt(111). Gray dots in (B) are experimental results taken from Ref. 66.

into three separate modes at 1250, 1020, and 997 cm^{-1} . The dynamic dipole moments of the latter two modes are nearly parallel to the surface, and hence they give only weak absorption in the surface spectra by the surface selection rule.

While those for bisulfate and hydronium-sulfate ion pair (not shown in this article) are far from the experiments,⁽⁵³⁾ the calculated spectra for adsorbed sulfate agree well with experimentally-obtained spectra reported in the literatures.⁽⁶⁶⁾ The calculation, therefore, can be concluded to support the hypothesis of sulfate as a dominant specie in a wide potential range.

Potential-dependences of the theoretically-obtained vibration frequencies for adsorbed sulfate also agree well with the experimental results⁽⁶⁶⁾ as shown in Fig. 9(B). The 1250 cm^{-1} band is significantly blue-shifted, while the 950 cm^{-1} band is slightly red-shifted when the electrode potential is increased. Our group⁽⁶⁷⁾ showed recently that the potential-dependent frequency changes are due to the so-called physical Stark effect, in which the vibrational changes are fully described by classical electrostatic interactions between dipole moments of adsorbed sulfate and external electric field across the electric double layer.

As illustrated in this subsection, theoretical simulations on vibrational spectra and their comparisons with experiments can give significant information to determine dominant adsorbates on electrode surfaces, and further analysis on potential-dependent vibration frequencies using theoretically-obtained vibrational modes can give further insights into details of adsorbate structures and their charge distributions.

3. 6 In situ X-ray Absorption Spectroscopy

3. 6. 1 Method

X-ray absorption spectroscopy (XAS) is also a powerful experimental method to examine structures of adsorbates at electrified interfaces,⁽⁶⁸⁻⁷⁰⁾ and the DFT-MPB method, again, can provide spectral information

In our implementation, an X-ray absorption cross section σ_s is calculated by a methodology using a projector-augmented-wave (PAW) method suggested by Taillefumier et al.,⁽⁷¹⁾ in which σ_s is described as follows:

$$\sigma_s(h\omega) = 4\pi\alpha_0 h\omega \sum_f |M_{i \rightarrow f}|^2 \delta(E_f - E_i - h\omega) \quad \dots \dots \dots (45)$$

$$M_{i \rightarrow f} \cong \sum_{\sigma} \sum_n \sum_l \sum_{m=-l}^l \langle \psi_{f\sigma}^{PP} | \phi_{n,l,m}^{AE} \rangle \langle \xi_{n,l,m}^{PP} | D | \psi_{i\sigma}^{AE} \rangle \quad \dots \dots \dots (46)$$

$$D = \boldsymbol{\varepsilon} \cdot \mathbf{r} \left(1 + \frac{i}{2} \mathbf{k} \cdot \mathbf{r} \right) \quad \dots \dots \dots (47)$$

where $h\omega$ is the photon energy; α_0 is the fine structure constant; $M_{i \rightarrow f}$ is the transition amplitude between an initial core state i with energy E_i and final state f with energy E_f ; $|\psi_{i\sigma}^{AE}\rangle$ and $|\psi_{f\sigma}^{PP}\rangle$ are the all electron wave function for the initial core state and the pseudo-wave function for the final state, respectively, with spin state σ , $|\phi_{n,l,m}^{AE}\rangle$ and $|\xi_{n,l,m}^{PP}\rangle$ are the all electron partial wave function and projector function specified by a principal number n , angular momentum number l and magnetic momentum number m ; D is the transition operator of the photon beam with a polarization vector $\boldsymbol{\varepsilon}$ and wave vector \mathbf{k} . Similarly to calculations described in previous sections, the final state wave function $|\psi_{f\sigma}^{PP}\rangle$ and its energy E_f are calculated changing the number of electrons, and σ_s is calculated on each of charged states. In the calculations of $|\psi_{f\sigma}^{PP}\rangle$ and E_f , a core-hole is introduced into a pseudopotential of an excited atom to include final state effects on XAS, and spin-orbit interactions are included within a perturbation scheme.⁽⁷²⁾

3. 6. 2 Results on X-ray Absorption Spectra of Pt(111)

Figure 10 summarizes the calculated L3 edges of Pt(111) with various adsorbates and surface charges. The height and position (energy) of the first peak increase with the increase in the surface coverage of OH or O as shown in Fig. 10(A), while the change in the surface charge does not contribute to the spectra if the surface coverage does not change as shown in Fig. 10(B). The result indicates that effects by the double layer charging are negligibly small contrarily to the experimental suggestion described in Ref. 69.

Figure 11 shows the height and position of the first peak as functions of the average valency of surface Pt

atoms. Both height and energy monotonously increase with the increase in the valency regardless the types of the surface (hydr)oxides. The result validates the conventional empirical method⁽⁶⁹⁾ to estimate the valence state of surface Pt atoms by interpolating the peak heights or positions of a few reference samples, such as metallic Pt and PtO₂. The result also indicates that neither structural nor compositional information can be obtained from the height and position of the first peak. For obtaining the information, spectra in higher energy region must be examined. For detecting subsurface oxides, for example, depressions in the intensity, which appear from 11553 to 11565 eV in the spectra of PtO₂/Pt(111) can be a good indicator.

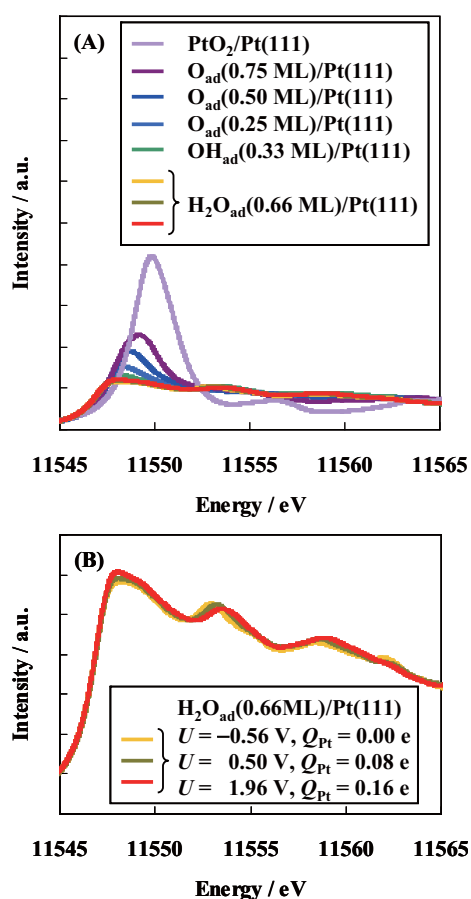


Fig. 10 Simulated X-ray absorption spectra of L3 edges of surface Pt atoms. (B) is the results on a Pt(111) surface covered by 0.66 ML of H₂O with H-up structure at different electrode potentials (or charged states). Q_{Pt} in (A) is an average charge per surface Pt atom.

4. Conclusions

Basic equations of the DFT-MPB and their recent applications to interfacial electrochemistry are presented in this article. By including electric double layers into DFT-based interfacial models, a variety of electrochemical properties are obtained on reaction free energies, electrosorption valency values, potential-dependent activation free energies, transfer coefficients (or Tafel slopes), transition state structures, potential-dependent vibrational frequencies and potential-dependent X-ray absorption spectroscopy. The developed method is a powerful tool to understand mechanisms of electrode reactions and to design new electrode materials for electrochemical power devices.

Acknowledgement

We thank Professor Alfred B. Anderson of Case Western Reserve University for many valuable advices on quantum chemical calculations of electrode reactions and Professor Masatoshi Osawa of Hokkaido University for his helpful advices on interpretations of IR-absorption spectra. We acknowledge also NEDO (New Energy and Industrial Technology Development Organization)

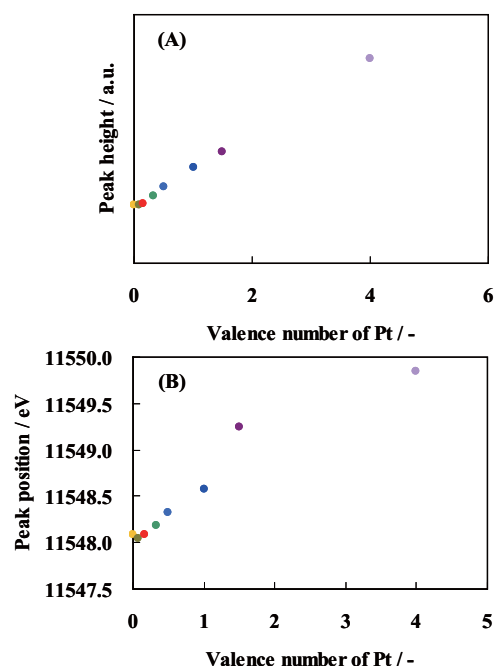


Fig. 11 Peak height (A) and position (B) as functions of an average valency of surface Pt atoms.

for their partial financial support. Dr. Ryoji Asahi, Mr. Akihiro Nagoya and Dr. Kazutoshi Miwa of Toyota Central R&D Labs., Inc. provided their theoretical data on X-ray absorption spectra, and Mr. Tatsuya Yoshida and Dr. Masahiko Mizuno of Toyota Central R&D Labs., Inc. helped to provide computational resources.

References

- (1) Butler, J. A. V., "Studies in Heterogeneous Equilibria. Part II.—The Kinetic Interpretation of the Nernst Theory of Electromotive Force", *Trans. Faraday Soc.*, Vol. 19 (1924), pp. 729-733.
- (2) Marcus, R. A., "On the Theory of Oxidation-Reduction Reactions Involving Electron Transfer. V. Comparison and Properties of Electrochemical and Chemical Rate Constants", *J. Phys. Chem.*, Vol. 67 (1963), pp. 853-857.
- (3) Trasatti, S., "Structure of the Metal Electrolyte Solution Interface - New Data for Theory", *Electrochim. Acta*, Vol. 36 (1991), pp. 1657-1658.
- (4) Bockris, J. O'M. and Khan, S. U. M., *Surface Electrochemistry: A Molecular Level Approach* (1993), Plenum Press.
- (5) Schmickler, W. and Santos, E., *Interfacial Electrochemistry, 2nd Edition* (1996), Springer.
- (6) Hohenberg, P. and Kohn, W., "Inhomogeneous Electron Gas", *Phys. Rev.*, Vol. 136 (1964), pp. B864-871.
- (7) Kohn, W. and Sham, L. J., "Self-consistent Equation Including Exchange and Correlation Effects", *Phys. Rev.*, Vol. 140 (1965), pp. A1133-A1138.
- (8) Parr, R. G. and Yang, W. T., *Density Functional Theory of Atoms and Molecules* (1989), Oxford Univ. Press.
- (9) Chong, D. P., Ed., *Recent Advances in Density Functional Methods* (1995), World Scientific.
- (10) Martin, R. M., *Electronic Structure: Basic Theory and Practical Methods* (2004), Cambridge University Press.
- (11) Gouy, G., "Sur la Constitution de la Charge Electrique à la Surface d'un Electrolyte", *J. Phys.*, Vol. 9 (1910), pp. 457-468.
- (12) Chapman, D. L., "A Contribution to the Theory of Electrocapillarity", *Philos. Mag.*, Vol. 25 (1913), pp. 475-481.
- (13) Debye, P. and Falkenhagen, H., "Dispersion of the Conductivity and Dielectric Constants of Strong Electrolytes", *Phys. Z.*, Vol. 29 (1928), pp. 121-132.
- (14) Guidelli, R. and Schmickler, W., "Recent Developments in Models for the Interface between a Metal and an Aqueous Solution", *Electrochim. Acta*, Vol. 45 (2000), pp. 2317-2338.
- (15) Lozovoi, A. Y., Alavi, A., Kohanoff, J. and Lynden-Bell, R. M., "Ab initio Simulation of Charged Slabs at Constant Chemical Potential", *J. Chem. Phys.*, Vol. 115 (2001), pp. 1661-1669.
- (16) Otani, M. and Sugino, O., "First-principles Calculations of Charged Surfaces and Interfaces: A Plane-wave Nonrepeated Slab Approach", *Phys. Rev. B*, Vol. 73 (2006), 115407.
- (17) Borukhov, I. and Andelman, D., "Steric Effects in Electrolytes: A Modified Poisson-Boltzmann Equation", *Phys. Rev. Lett.*, Vol. 79 (1997), pp. 435-438.
- (18) Borukhov, I., Andelman, D. and Orland, H., "Adsorption of Large Ions from an Electrolyte Solution: A Modified Poisson-Boltzmann Equation", *Electrochim. Acta*, Vol. 46 (2000), pp. 221-229.
- (19) Jinnouchi, R. and Anderson, A. B., "Electronic Structure Calculations of Liquid-solid Interfaces: Combination of Density Functional Theory and Modified Poisson-Boltzmann Theory", *Phys. Rev. B*, Vol. 77 (2008), 245417.
- (20) Jinnouchi, R. and Anderson, A. B., "Aqueous and Surface Redox Potentials from Self-consistently Determined Gibbs Energies", *J. Phys. Chem. C*, Vol. 112 (2008), pp. 8747-8750.
- (21) Fattebert, J.-L. and Gygi, F., "First-principles Molecular Dynamics Simulations in a Continuum Solvent", *Int. J. Quantum Chem.*, Vol. 93 (2003), pp. 139-147.
- (22) Scherlis, D. A., Fattebert, J.-L., Gygi, F., Cococcioni, M. and Marzari, N., "A Unified Electrostatic and Cavitation Model for First-principles Molecular Dynamics in Solution", *J. Chem. Phys.*, Vol. 124 (2006), 074103.
- (23) Born, M. and Oppenheimer, J. R., "Zur Quantentheorie der Molekeln", *Ann. Phys.*, Vol. 84 (1927), pp. 457-484.
- (24) Steinfeld, J. I., Francisco, J. S. and Hase, W. L., *Chemical Kinetics and Dynamics* (1989), Prentice Hall, Englewood Cliffs, NJ.
- (25) Szabo, A. and Ostlund, N., *Modern Quantum Chemistry: Introduction to Advanced Electronic Structure Theory* (1996), Dover.
- (26) Miertuš, S., Scrocco, E. and Tomasi, J., "Electrostatic Interaction of a Solute with a Continuum. A Direct Utilization of ab initio Molecular Potentials for the Prevision of Solvent Effects", *Chem. Phys.*, Vol. 55 (1981), pp. 117-129.
- (27) Cramer, C. J. and Truhlar, D. G., "General Parameterized SCF Model for Free Energies of Solvation in Aqueous Solution", *J. Am. Chem. Soc.*, Vol. 113 (1991), pp. 8305-8311.
- (28) Chandrasekhar, J. and Jorgensen, W. L., "Energy Profile for a Non-concerted SN2 Reaction in Solution", *J. Am. Chem. Soc.*, Vol. 107 (1985), pp. 2974-2975.
- (29) Kovalenko, A. and Hirata, F., "Self-consistent Description of a Metal-water Interface by the Kohn-Sham Density Functional Theory and the Three-Dimensional Reference Interaction Site Model", *J. Chem. Phys.*, Vol. 110 (1999), pp. 10095-10111.
- (30) Mermin, N. D., "Thermal Properties of the

- Inhomogeneous Electron Gas”, *Phys. Rev.*, Vol. 137 (1965), pp. A1441-A1443.
- (31) Bonnet, N., Morishita, T., Sugino, O. and Otani, M., “First-principles Molecular Dynamics at a Constant Electrode Potential”, *Phys. Rev. Lett.*, Vol. 109 (2012), 266101.
- (32) van Santen, R. A. and Niemantsverdriet, H. J. W., *Chemical Kinetics and Catalysis (Fundamental and Applied Catalysis)* (1995), Plenum.
- (33) Fu, C.-L. and Ho, K.-M., “First-principles Calculation of the Equilibrium Ground-state Properties of Transition Metals: Applications to Nb and Mo”, *Phys. Rev. B*, Vol. 28 (1983), pp. 5480-5486.
- (34) Farkas, Ö. and Schlegel, H. B., “Methods for Optimizing Large Molecules. II. Quadratic Search”, *J. Chem. Phys.*, Vol. 111 (1999), pp. 10806-10814.
- (35) Payne, M. C., Teter, M. P., Allan, D. C., Arias, T. A. and Joannopoulos, J. D., “Iterative Minimization Techniques for ab initio Total-energy Calculations: Molecular Dynamics and Conjugate Gradients”, *Rev. Mod. Phys.*, Vol. 64 (1992), pp. 1045-1097.
- (36) Becke, A. D., “A Multicenter Numerical Integration Scheme for Polyatomic Molecules”, *J. Chem. Phys.*, Vol. 88 (1988), pp. 2547-2553.
- (37) Delley, B., “An All-electron Numerical Method for Solving the Local Density Functional for Polyatomic Molecules”, *J. Chem. Phys.*, Vol. 92 (1990), pp. 508-517.
- (38) Adams, L. and Xie, D., “New Parallel SOR Method by Domain Partitioning”, *SIAM J. Sci. Comput.*, Vol. 20 (1999), pp. 2261-2281.
- (39) Brandt, A., “Multi-level Adaptive Solutions to Boundary-value Problems”, *J. Math. Comp.*, Vol. 31 (1977), pp. 333-390.
- (40) Stroud, A. H., *Approximate Calculation of Multiple Integrals* (1971), Prentice-Hall.
- (41) Treutler, O. and Ahlrichs, R., “Efficient Molecular Numerical Integration Schemes”, *J. Chem. Phys.*, Vol. 102 (1994), pp. 346-354.
- (42) Marković, N. M., Schmidt, T. J., Grgur, B. N., Gasteiger, H. A., Behm, R. J. and Ross, P. N., “Effect of Temperature on Surface Processes at the Pt(111)-liquid Interface: Hydrogen Adsorption, Oxide Formation, and CO Oxidation”, *J. Phys. Chem. B*, Vol. 103 (1999), pp. 8568-8577.
- (43) Tian, F., Jinnouchi, R. and Anderson, A. B., “How Potentials of Zero Charge and Potentials for Water Oxidation to OH(ads) on Pt(111) Electrodes Vary with Coverage”, *J. Phys. Chem. C*, Vol. 113 (2009), pp. 17484-17492.
- (44) Anderson, A. B., Uddin, J. and Jinnouchi, R., “Solvation and Zero-point-energy Effects on OH(ads) Reduction on Pt(111) Electrodes”, *J. Phys. Chem. C*, Vol. 114 (2010), pp. 14946-14952.
- (45) Jinnouchi, R., Kodama, K., Hatanaka, T. and Morimoto, Y., “First Principles-based Mean Field Model of Oxygen Reduction Reaction”, *Phys. Chem. Chem. Phys.*, Vol. 13 (2011), pp. 21070-21083.
- (46) Tian, F. and Anderson, A. B., “Effective Reversible Potential, Energy Loss, and Overpotential on Platinum Fuel Cell Cathodes”, *J. Phys. Chem. C*, Vol. 115 (2011), pp. 4076-4088.
- (47) Anderson, A. B., “Insights into Electrocatalysis”, *Phys. Chem. Chem. Phys.*, Vol. 14 (2012), pp. 1330-1338.
- (48) Anderson, A. B., Jinnouchi, R. and Uddin, J., “Effective Reversible Potentials and Onset Potentials for O₂ Electroreduction on Transition Metal Electrodes: Theoretical Analysis”, *J. Phys. Chem. C*, Vol. 117 (2013), pp. 41-48.
- (49) Gómez, R., Orts, J. M., Álvarez-Ruiz, B. and Feliu, J. M., “Effect of Temperature on Hydrogen Adsorption on Pt(111), Pt(110), and Pt(100) Electrodes in 0.1M HClO₄”, *J. Phys. Chem. B*, Vol. 108 (2004), pp. 228-238.
- (50) Gómez-Marín, A. M., Clavilier, J. and Feliu, J. M., “Sequential Pt(111) Oxide Formation in Perchloric Acid: An Electrochemical Study of Surface Species Inter-conversion”, *J. Electroanal. Chem.*, Vol. 688 (2013), pp. 360-370.
- (51) Clavilier, J., “Role of Anion on the Electrochemical-behavior of a (111) Platinum Surface - Unusual Splitting of the Voltammogram in the Hydrogen Region”, *J. Electroanal. Chem.*, Vol. 107 (1980), pp. 211-216.
- (52) Kolics, A. and Wieckowski, A., “Adsorption of Bisulfate and Sulfate Anions on a Pt(111) Electrode”, *J. Phys. Chem. B*, Vol. 105 (2001), pp. 2588-2595.
- (53) Jinnouchi, R., Hatanaka, T., Morimoto, Y. and Osawa, M., “First Principles Study of Sulfuric Acid Anion Adsorption on a Pt(111) Electrode”, *Phys. Chem. Chem. Phys.*, Vol. 14 (2012), pp. 3208-3218.
- (54) Herrero, E., Buller, L. J. and Abruña, H. D., “Underpotential Deposition at Single Crystal Surfaces of Au, Pt, Ag and Other Materials”, *Chem. Rev.*, Vol. 101 (2001), pp. 1897-1930.
- (55) Wu, Z.-W., Zang, Z.-H. and Yau, S.-L., “Electrodeposition of Copper at Well-defined Pt(111) and Rh(111) Electrodes in Sulfuric Acid Solution: Studying with in situ Scanning Tunneling Microscopy”, *Langmuir*, Vol. 16 (2000), pp. 3522-3528.
- (56) Jinnouchi, R., Hatanaka, T. and Morimoto, Y., “First Principles Study on Underpotential Deposition of Cu on Single Crystal Surfaces”, *Spring Meeting of the Electrochemical Society of Japan*, (2011), p. 1F08.
- (57) Trasatti, S. and Parsons, R., “Interphases in Systems of Conducting Phases”, *J. Electroanal. Chem.*, Vol. 205 (1986), pp. 359-376.
- (58) Frenkel, D. and Smit, B., *Understanding Molecular Simulation* (1996), Academic Press.
- (59) Janak, J. F., “Proof that $\partial E/\partial n_i = \epsilon_i$ in Density-functional Theory”, *Phys. Rev. B*, Vol. 18 (1978), pp. 7165-7168.
- (60) Henkelman, G., Uberuaga, B. P. and Jónsson, H., “A Climbing Image Nudged Elastic Band Method for

- Finding Saddle Points and Minimum Energy Paths”, *J. Chem. Phys.*, Vol. 113 (2000), pp. 9901-9904.
- (61) Maragakis, P., Andreev, S. A., Brumer, Y., Reichman, D. R. and Kasiras, E., “Adaptive Nudged Elastic Band Approach for Transition State Calculation”, *J. Chem. Phys.*, Vol. 117 (2002), pp. 4651-4658.
- (62) Henkelman, G. and Jónsson, H., “A Dimmer Method for Finding Saddle Points on High Dimensional Potential Surfaces Using Only First Derivatives”, *J. Chem. Phys.*, Vol. 111 (1999), pp. 7010-7022.
- (63) Atkins, P. and de Paula, J., *Physical Chemistry* (2006), Oxford University Press.
- (64) Ito, M., “Structures of Water at Electrified Interfaces: Microscopic Understanding of Electrode Potential in Electric Double Layers on Electrode Surfaces”, *Surf. Sci. Rep.*, Vol. 63 (2008), pp. 329-389.
- (65) Nichols, R. J., *Adsorption of Molecules at Metal Electrodes*, Lipkowsky, J. and Ross, P. N., Eds., (1992), pp. 347-390, VCH Publishers.
- (66) Lachenwitzer, A., Li, N. and Lipkowsky, J., “Determination of the Acid Dissociation Constant for Bisulfate Adsorbed at the Pt(111) Electrode by Subtractively Normalized Interfacial Fourier Transform Infrared Spectroscopy”, *J. Electroanal. Chem.*, Vol. 532 (2002), pp. 85-98.
- (67) Jinnouchi, R., Hatanaka, T., Morimoto, Y. and Osawa, M., “Stark Effect on Vibration Frequencies of Sulfate on Pt(111) Electrode”, *Electrochim. Acta*, Vol. 101 (2013), pp. 254-261.
- (68) Mukerjee, S., Srinivasan, S., Soriaga, M. P. and McBreen, J., “Effect of Preparation Conditions of Pt Alloys on Their Electronic, Structural, and Electrocatalytic Activities for Oxygen Reduction-XRD, XAS, Electrochemical Studies”, *J. Phys. Chem.*, Vol. 99 (1995), pp. 4577-4589.
- (69) Tada, M., Shigeki, M., Asaoka, T., Hiroshima, K., Okumura, K., Tanida, H., Uruga, T., Nakanishi, H., Matsumoto, S., Inada, Y., Nomura, M. and Iwasawa, Y., “In situ Time-resolved Dynamic Surface Events on the Pt/C Cathode in a Fuel Cell under Operando Conditions”, *Angew. Chem. Int. Ed.*, Vol. 46 (2007), pp. 4310-4315.
- (70) Imai, H., Izumi, K., Matsumoto, M., Kubo, Y., Kato, K. and Imai, Y., “In situ and Real-time Monitoring of Oxide Growth in a Few Monolayers at Surfaces of Platinum Nanoparticles in Aqueous Media”, *J. Am. Chem. Soc.*, Vol. 131 (2009), pp. 6293-6300.
- (71) Tailliefumier, M., Cabaret, D., Flank, A.-M. and Mauri, F., “X-ray Absorption Near-edge Structure Calculations with the Pseudopotentials: Application to the K Edge in Diamond and α -quartz”, *Phys. Rev. B*, Vol. 66 (2002), 195107.
- (72) Hamstreet, L. A., Fong, C. Y. and Nelson, J. S., “First-principles Calculations of Spin-orbit Splittings in Solids Using Nonlocal Separable Pseudopotentials”, *Phys. Rev. B*, Vol. 47 (1993), pp. 4238-4243.

Ryosuke Jinnouchi

Research Fields:

- Computational Physics
- Electrochemistry

Academic Degree: Dr.Eng.

Academic Society:

- The Electrochemical Society of Japan

**Kensaku Kodama**

Research Field:

- Electrochemistry

Academic Society:

- The Electrochemical Society of Japan

**Eishiro Toyoda**

Research Fields:

- Surface Science
- Electrochemistry

Academic Societies:

- The Physical Society of Japan
- The Electrochemical Society of Japan

**Yu Morimoto**

Research Fields:

- Electrochemistry
- Fuel Cell Engineering

Academic Degree: Ph.D.

Academic Societies:

- The Electrochemical Society of Japan
- The Committee of Battery Technology
- The Electrochemical Society

